CrystEngComm

Accepted Manuscript

ROYAL SOCIETY OF CHEMISTRY

www.rsc.org/crystengcomm

Journal Name

RSCPublishing

ARTICLE

Structure Determination of Theophylline-Nicotinamide Cocrystal: A Combined Powder XRD, 1D Solid-State NMR, and Theoretical Calculation Study

Cite this: DOI: 10.1039/xoxxoooooox

Received ooth January 2012,
Accepted ooth January 2012

DOI: 10.1039/xoxxoooooox

www.rsc.org/

Ping Li,[a,b,§] Yueying Chu,[c,§] LinWang,[a] Robert M. Wenslow Jr.,[d] Kaichao Yu,[b] Hailu Zhang*[a] and Zongwu Deng[a]

The crystal structure of a powder pharmaceutical cocrystal, theophylline-nicotinamide (1:1) crystal complex, is solved for the first time by using a combination of X-ray powder diffraction (XRPD), 1D solid state NMR, as well as density functional theory (DFT) calculations. With the aid of solid state NMR spectroscopy, a candidate structure can be determined from XRPD data by Rietveld refinement with acceptable residual variances. The structure was subjected to periodic geometry optimization, followed by NMR parameter calculations. The agreement between experimental and computed ^{13}C and ^{15}N NMR chemical shift values validates the refined structure as an accurate representation of the actual cocrystal structure. Intermolecular interactions existing in the cocrystal are further confirmed by the commonly used vibrational spectra. This study confirms the straightforward synergistic approach offers a simple and credible way to solve the crystal structure of powder cocrystal samples.

Introduction

A cocrystal is a structurally homogeneous crystalline complex, simultaneously containing two or more components that are solids at ambient condition in a well-defined stoichiometry, where at least one cocrystal former is in an un-ionized state.[1-3] In recent years, cocrystals have been widely used as means to improve and tailor the physicochemical properties of active pharmaceutical ingredients (APIs), such as thermal stability, mechanical properties, dissolution rate, solubility, hygroscopicity, and chiral resolution.[4-9] For pharmaceutical cocrystals, studies reveal that some physicochemical properties (e.g. solubility, tabletting properties, thermal and hydration stability) can be readily predicted by crystal structures in addition to corresponding properties of the constituents.[10,11] Thus, the understanding of structure-property relationships is necessary as research strives towards synthesis by design.

For structure investigations, qualified single crystals are typically desired. However, the preparation of satisfactory single crystal samples of cocrystals is often restricted by many factors, i.e. the different solubilities of the cocrystal formers during the most prevalent solution cocrystallisation processes.[12] In comparison, it is more efficient and convenient for researchers to obtain cocrystal powder samples by various routes including neat grinding[13] and solvent-drop grinding[14]. These methods would then require obtaining a crystal structure from the powder sample. Fortunately, the development of X-ray powder diffraction (XRPD) equipment and structure solving algorithms make it possible to extract crystal structure from the XRPD pattern.[12,15] However, due to the highly overlapped Bragg peaks and limited data, the structural information extracted from XRPD pattern is often not a true representation of actual structure. Thus, it is further necessary to confirm the refined result via other methods. Solid state NMR spectroscopy (ssNMR), which provides information concerning the chemical environment of organic nuclei (e.g. ^{1}H, ^{13}C, $^{14/15}N$, ^{19}F, ^{31}P), can provide this supplementary structure information. The combination of XRPD and ssNMR to solve structure of pharmaceutical crystals can be found in several reports which mainly focus on pure API.[16,17] Recently, peers also introduced such a protocol into the cocrystal field.[18]

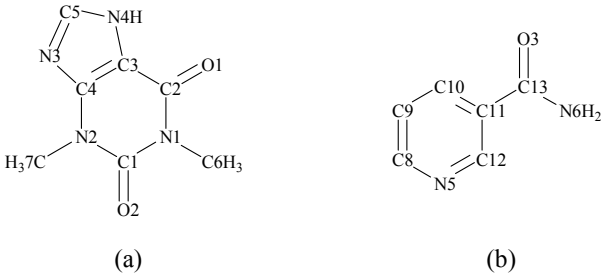

Scheme 1 Molecular structures of TP (a) and NCT (b).

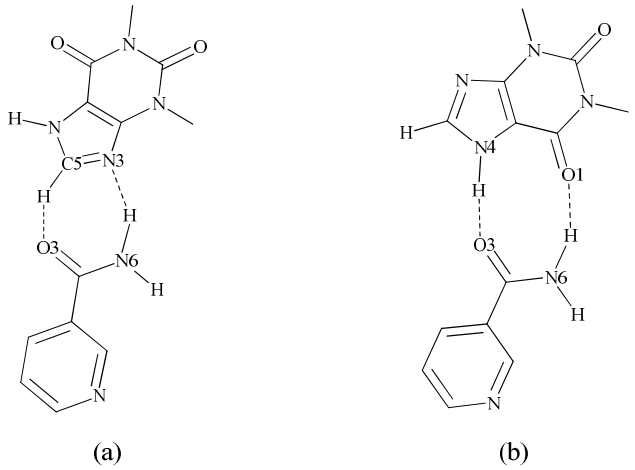

Scheme 2 Two proposed heterosynthons between TP and NCT.

In this study, the crystal structure of a powder pharmaceutical cocrystal of theophylline (TP) and nicotinamide (NCT) (Scheme 1) is determined by a combination of XRPD, 1D ssNMR, and density functional theory (DFT) calculations. The preparation of 1:1 TP-NCT cocrystal was first reported by Lu and Rohani with improved physicochemical properities.[19] According to the Raman data, an $R_2^2(7)$ supramolecular synthon (Scheme 2a) was proposed existing in the cocrystal, where intermolecular hydrogen bondings occur between N3, C5−H of TP and amide of NCT.[19] A similar $R_2^2(7)$ graph set can be observed when caffeine (structural analogue of TP) cocrystallized with some organic carboxylic acids.[8] According to the hydrogen-bond rules for organic compounds,[20] the primary synthons always formed between best acceptor and best donor. Hence, $R_2^2(9)$ synthon shown in Scheme 2b is expected to be established between TP and NCT molecules. Such $R_2^2(9)$ graph set (or its analogues) can be observed when TP cocrystallized with urea,[21] organic carboxylic acids,[22-25] and other molecules[26]. Additionally, dimeric interactions formed between two TP molecules (an analogue of Scheme 2b) may also exist.[27-29] It is critical to ensure which kind of supramolecular synthon exists in the TP-NCT cocrystal, and whether novel supramolecular synthon can be found.

Experimental

Materials and sample preparation

TP (≥99%, Adamas Reagent Co., Ltd., China), NCT (≥98.5%, Sinopharm Chemical Reagent Co., Ltd., China) and EtOH (≥99.7%, Sinopharm Chemical Reagent Co., Ltd., China) were purchased and used as received. In order to obtain the TP-NCT cocrystal, 72 mg TP was ground with 48.8 mg NCT (in a molar ratio of 1:1) in a pestle and mortar for 10 min followed by addition of one drop of EtOH, then the resulting mixture was further ground for 20 min. Single crystal growth was also attempted by using solution methods, but no sample with appropriate size and quality was obtained for further single-crystal X-ray diffraction analysis.

X-ray powder diffraction

XRPD data were collected on a PANalytical X'Pert Pro X-ray powder diffractometer (PANalytical B.V., Almelo, The Netherlands) equipped with X'Celerator Real Time Mutil-Strip detector. A Cu Kα radiation was used at 45 kV and 40 mA. Samples were wrapped in two pieces of Mylar film and scanned in the transmission mode. The scan range, step size, and time per step were 2θ = 3.0 to 40.0°, 0.0167113°, and 30 s, respectively.

Vibrational (Raman and FTIR) spectroscopy

Raman analyses were performed by using a LabRam HR 800 confocal Raman system (HORIBA, Ltd., Lille, France) in the spectral range of 400–4000 cm^{-1}. The excitation of Raman scattering was operated by a He−Ne laser at 632.81 nm. Samples were placed on glass with acquisition time of 20 s. FTIR spectra were collected on a Thermo-Nicolet 6700 IR spectrometer (Thermo Fisher Scientific, Waltham, MA). Samples were compressed into disks with KBr and analyzed over the wavenumber range of 400–4000 cm^{-1} with 100 scans at a resolution of 4 cm^{-1}.

Solid-state NMR (^{13}C NMR and ^{15}N NMR)

Solid-state ^{13}C and ^{15}N cross-polarization magic angle spinning (CP/MAS) spectra were acquired using a Bruker AVANCE III-500 spectrometer (Bruker BioSpin, Karlsruhe, Germany) operating at a magnetic field strength of 11.7 T, equipped with a 4 mm double-resonance MAS probe. A total of sideband suppression (TOSS) frame was embedded into the conventional Cross-Polarization (CP) pulse sequence, which was used to acquire the ^{13}C and ^{15}N CP/MAS spectra. The Hartmann-Hahn conditions of the CP/MAS TOSS experiment for acquiring ^{13}C and ^{15}N spectra were optimized by using adamantane and glycine, respectively. ^{13}C NMR spectra were obtained at an 8 kHz MAS spinning speed with a contact time of 2 ms. ^{15}N NMR spectra were obtained at an 8 kHz MAS spinning speed with a contact time of 3.5 ms. Recycle delay times for TP, NCT, and cocrystal are 10 s, 200 s, and 10 s, respectively. In order to make a distinction between protonated carbon atoms and quaternary carbon atoms, the non-quaternary carbon suppression (^{13}C NQS) experiment of cocrystal was also performed. ^{13}C, ^{15}N chemical shifts were externally referenced to adamantane (δ = 29.5 ppm) and L-glycine (δ = −347.0 ppm), respectively.

Computation methods

All the computational tasks were performed using *Accelrys Materials studio (MS)* software. The cocrystal structure refinement from XRPD was carried out using *MS Reflex* program. After completing pattern processing, the diffraction pattern was first indexed by using the TREOR90 algorithm[30]. Next, Pawley refinement[31] of the peak profiles was performed until the figure of merit reached a good quality of fit (R_{wp} = 3.01%, R_p = 2.28%). Subsequently, a couple of TP and NCT molecules were introduced into the empty unit cell determined

by the Pawley refinement. This structure model was subjected to preliminary crystal structure solution using a direct-space method based on the Simulated Annealing algorithm. The best fit between the simulated and experimented powder patterns was obtained with R_{wp} = 7.25% (R_p = 5.32%). The obtained structure model was used for the final Rietveld refinement.[32]

The TP (CSD refcode: BAPLOT01)[33], NCT (CSD refcode: NICOAM02)[34], and refined cocrystal structures were subjected to first-principles geometry optimization to obtain configurations with minimum energy by keeping the unit cell parameters fixed while allowing the positions of all atoms to be relax freely. Such optimization can help to obtain more accurate atomic coordinates in the crystal cell, from which more accurate chemical shift values can be derived.[35,36] Optimizations were performed by using the *MS CASTEP* program which implements density functional theory within a generalized gradient approximation (GGA) and the planewave pseudopotential approach.[37] Calculations were carried out by using Perdew-Burke-Ernzerhof (PBE) functional, ultrasoft pseudopotential, medium planewave cutoff energy (300 eV) and K-point as default setting in MS package. NMR shielding calculations were performed with *MS CASTEP-NMR* code, using periodic gauge including projector augmented waves (GIPAW) method at the GGA/PBE level. A fine K-point and cut-off energy of 550 eV were employed, combining with core-valance interactions described by ultrasoft pseudopotential generated on-the-fly.

Results and discussion

Cocrystal characterization

The preparation of 1:1 TP-NCT cocrystal was first reported by Lu and Rohani.[19] The TP-NCT sample obtained in this study was first characterized by XRPD and differential scanning calorimetry. The resulting XRPD pattern and melting point agree well with the reference (Supporting Information: Figure S1&S2),[19] indicating successful synthesis of the target product.

The cocrystal was further characterized by ^{13}C CP/MAS TOSS NMR (Fig. 1c). ^{13}C chemical shifts of TP and NCT (Fig. 1a and 1b) can be clearly assigned according to ref. [38] and [39]. The TP-NCT sample shows slight changes in ^{13}C chemical shifts with respect to the spectra of input materials, which is ascribed to the altered chemical environments associated with the formation of a new phase. Chemical shifts of C3, C5, C6, C7, C9, C10, C11, and C13 in the new phase can be assigned directly by referring to the spectra of TP and NCT. The remaining peaks are assigned with the help of NQS data (Figure 1d). Each chemically distinct carbon in the cocrystal molecule is represented by single resonance, and no peaks of phase impurities can be found in the ^{13}C spectrum. Thus, it's easy to realize the resulting phase is not a physical mixture of input materials, nor does it contain impurities at detectable concentrations, and the number of molecules per asymmetric unit (Z') should be equal to 1 for the cocrystal. ^{15}N solid state NMR spectra of TP, NCT, and cocrystal were also collected (Supporting Information: Figure S3). The resonance peaks of cocrystal sample can be readily assigned by referring to that of the input materials.[40]

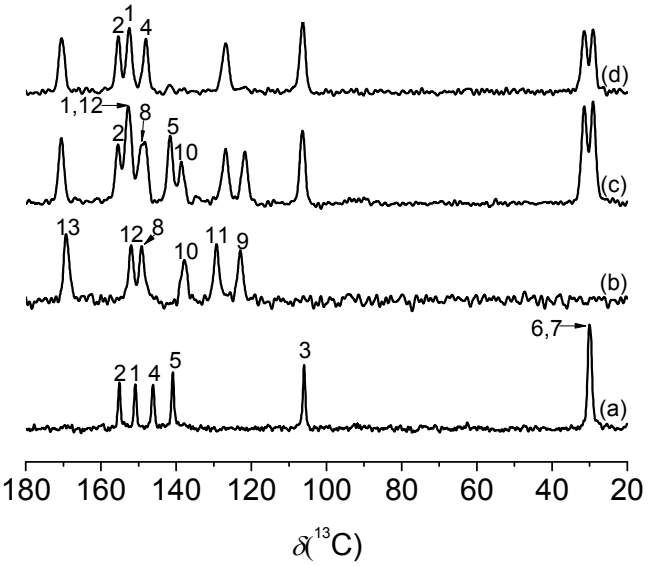

Figure 1 ^{13}C CP/MAS TOSS NMR spectra of TP (a), NCT (b), cocrystal (c) and ^{13}C NQS NMR spectrum of cocrystal (d).

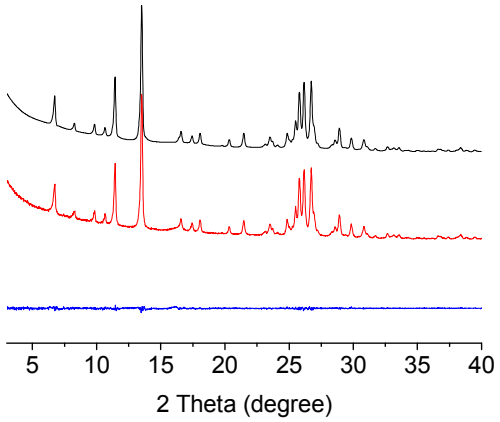

Figure 2 Restrained Rietveld fitting of the TP-NCT XRPD data, where the measured pattern is represented with the black line (top), the simulated pattern with the red line (middle), and the difference pattern with the blue line (bottom), respectively.

Structure determination from XRPD

Formation of cocrystals is dependent on the establishment of favorable non-covalent intermolecular interactions. As mentioned in the introduction section, there may be multiple possibilities, though the $R_2^2(9)$ heterosynthon (Scheme 2b) is most favorable. With the assistance of solid state NMR spectroscopy (Z' = 1), one cocrystal structure was determined from the XRPD data by Rietveld refinement with favorable residual variances (Figure 2, R_{wp} = 3.38%, R_p = 2.49%). Crystallographic details of the refined structure are presented in Table 1 and Table 2.

As shown in Figure 3 and Table 2, the refined structure mainly adopts the $R_2^2(9)$ heterosynthon (Scheme 2b) with a

TP/NCT ratio of 1:1. The TP-NCT cocrystal crystallizes in the monoclinic unit cell where each unit cell is comprised of four TP molecules and four NCT molecules. C2=O1 and N4−H of TP connect with amide group of NCT, forming a intermolecular hydrogen bonding pair, the surplus N6−H proton is further hydrogen bonded with the C1=O2 group of another TP molecule. Additionally, very weak dimeric interaction occurs between two NCT molecules via C8−H and N5 atoms, and N3 of TP is weakly interacted with C10−H of NCT.

Table 1 Crystallographic details of the refined cocrystal structure.

Name	TP-NCT cocrystal
Formula	C13H14N6O3
Molecular weight	302.30
Crystal system	monoclinic
Space group	P1 21/C1
a (Å)	3.8669
b (Å)	16.6497
c (Å)	21.7468
α (°)	90
β (°)	99.5215
γ (°)	90
Volume (Å3)	1380.830
Z/Z'	4/1
Rwp	3.38%
Rp	2.49%

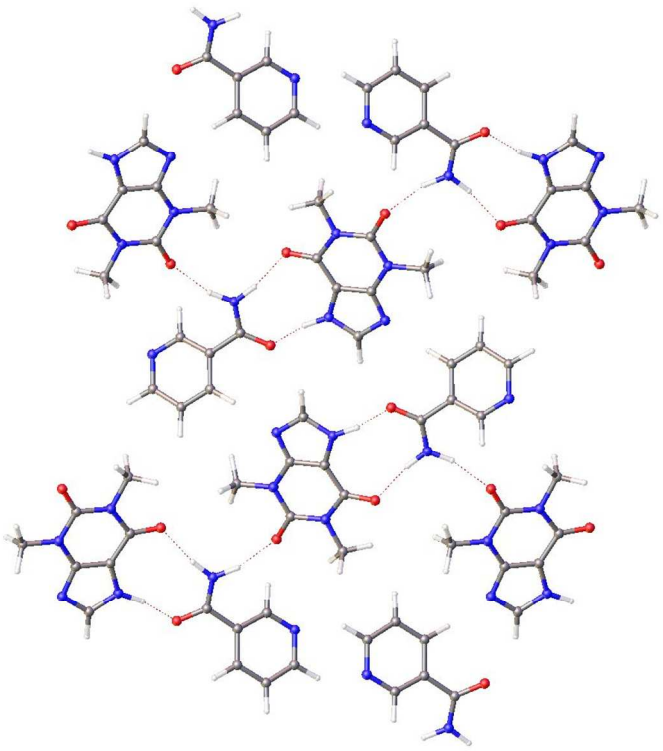

Figure 3 Packing diagram of refined cocrystal structure viewed along [100] face.

Table 2 Intermolecular hydrogen bonds in TP-NCT cocrystal

D−H···A	D−H/Å	H···A/Å	D···A/Å	D−H···A/deg
N4−H···O3	1.063(1.061[a])	1.774(1.704)	2.835(2.760)	176.032(173.786)
N6−H···O1	1.034(1.035)	2.004(1.922)	3.032(2.946)	172.473(169.584)
N6−H···O2	1.029(1.028)	1.922(1.987)	2.918(2.991)	161.687(164.600)
C8−H···N5	1.093(1.093)	2.545(2.476)	3.427(3.428)	137.049(144.706)
C10−H···N3	1.091(1.090)	2.412(2.511)	3.463(3.572)	161.009(163.962)

[a] the parameters after geometry optimization are shown in the brackets; TP-NCT structure after geometry optimization (in CIF format) can be found in Supporting Information.

Table 3 Experimental and calculated[a] $^{13}C/^{15}N$ chemical shifts of TP, NCT, and cocrystal.

Position	δ_{TP}^{exp}	δ_{TP}^{cal}	$\delta_{TP\text{-}NCT}^{exp}$	$\delta_{TP\text{-}NCT}^{cal}$	Position	δ_{NCT}^{exp}	δ_{NCT}^{cal}	$\delta_{TP\text{-}NCT}^{exp}$	$\delta_{TP\text{-}NCT}^{cal}$
C1	150.8	149.5	152.7	153.5	C8	149.2	152.6	149.1	149.5
N1	−226.6	−222.8	−230.8	−229.3	C9	122.9	124.1	121.7	120.1
C2	155.1	153.7	155.4	156.0	C10	137.9	138.5	138.6	136.1
C3	105.9	106.8	106.4	107.2	C11	129.3	131.3	126.8	127.8
C4	146.1	145.4	148.3	147.9	N5	−77.6[c]	−77.4	−66.5	−67.0
N2	−269.0	−265.8	−264.7	−263.3	C12	152.0	155.2	152.7	151.2
N3	−162.3	−167.6	−145.5	−146.7	C13	169.3	171.3	170.5	171.6
C5	140.9	140.5	141.5	141.9	N6	−275.8	−276.5	−274.4	−277.4
N4	−218.1	−219.2	−218.8	−222.8					
C6	30.0	25.3[b]	29.1	25.1					
C7			31.4	26.2					

[a] the calculated $^{13}C/^{15}N$ chemical shifts $\delta^{cal} = -(\sigma^{cal} - \sigma^{ref})$, where σ^{cal} is the calculated $^{13}C/^{15}N$ shielding value, σ^{ref} = 168.0 ppm (for ^{13}C) and −165.2 ppm (for ^{15}N), respectively; [b] average chemical shift value of C6&C7; [c] from ref.[45].

DFT calculations

Though the structure refinement is regarded as a routine practice,[41,42] it remains a trial-and-error approach. A solution

with acceptable XRPD feature of merit (R_{wp} and R_p) can not always ensure the correctness of the obtained structure. Following the recent examples,[16-18,43,44] NMR parameters are used to evaluate the rationality of the refined TP-NCT structure.

Experimental and calculated ^{13}C and ^{15}N chemical shift data of cocrystal and two input materials are summarized in Table 3. For TP and NCT, the maximal chemical shift difference between the experimental and calculated values is ca. 5 ppm, which is within the level of calculating error and confirms the availability of current computational accuracy. After the cocrystal formation, the experimental chemical shift changes of ^{13}C spins are all less than 2.5 ppm, while for some nitrogen atoms (N3 and N5), significant experimental chemical shift changes are observed. It's a normal phenomenon for nitrogen atoms but not carbon atoms are often directly involved in the intermolecular interaction changes. For the cocrystal sample, the calculated ^{13}C and ^{15}N chemical shifts (especially for ^{15}N spins) all agree well with the experimental values, indicating the refined structure is the accurate representation of actual cocrystal structure.

Further checking the intermolecular interactions

For N3 and N5 spins, the ^{15}N chemical shifts are displaced by 16.8 and 11.1 ppm after cocrystal formation, respectively. Significant differences of intermolecular interactions between the original materials and cocrystal sample on these sites are believed to be the major contributor of these large chemical shift variations.

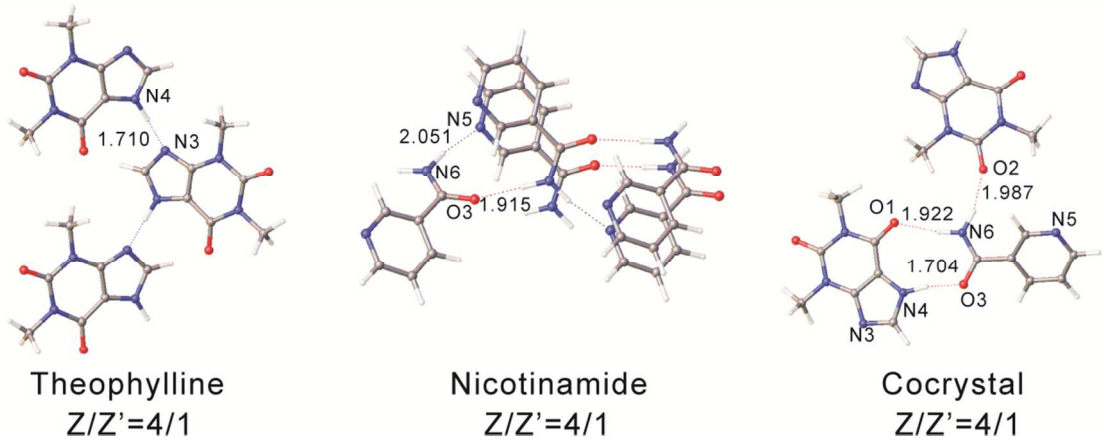

Figure 4 Intermolecular hydrogen bonds in TP (a), NCT (b), and TP-NCT cocrystal (c). The relevant inter-atomic distances are in Å.

Figure 4 displays the crystal fragments of TP, NCT, and cocrystal after periodic structure optimization. In TP crystal, N3 is involved in a strong hydrogen bond (1.710 Å) with N4−H of another TP molecule. In the cocrystal, O3 plays the role of proton acceptor as N3 does in TP crystal. While, N3 is only very weakly (2.511 Å) interacted with C10−H in the cocrystal form, leading to a significant de-shielding effect on the nuclear and hence a significant downfield ^{15}N chemical shift value.[46] N5 in the NCT molecule encounters a similar situation compared to N3. Such qualitative analysis displays consistency of intermolecular interaction changes and characteristic chemical shifts, further confirming the correctness of the obtained structure.

Once the crystal structure was confirmed, the commonly used Raman[19] and FTIR data should be investigated to check for consistency. RAMAN spectra of TP, NCT, and cocrystal are shown in Figure 5. The obvious changes (~10 cm^{-1}) of the C=O stretching frequency of TP[47] (from 1706&1664 to 1715&1673 cm^{-1}) suggest the carbonyl groups should be involved in hydrogen bonding in the cocrystal (Figure 4). For NCT, the change on its C=O stretching frequency[48] is inconspicuous (from 1677 to 1673 cm^{-1}), indicating the C13=O3 involved hydrogen bonding still exists in the cocrystal (Figure 4). For N4−H group of TP, Raman data only show there is no obvious alterations on its in-plane deformation mode (from 1249 to 1251 cm^{-1})[47]. The $N6H_2$ rocking frequency of NCT is very weak[48] (Figure 5b), and therefore a clear assignment in the spectrum of cocrystal sample is difficult. In the high wavenumber range (> 2750 cm^{-1}), Raman spectra only show the activity of C−H stretching[47,48], while information concerning N−H stretching is absent.

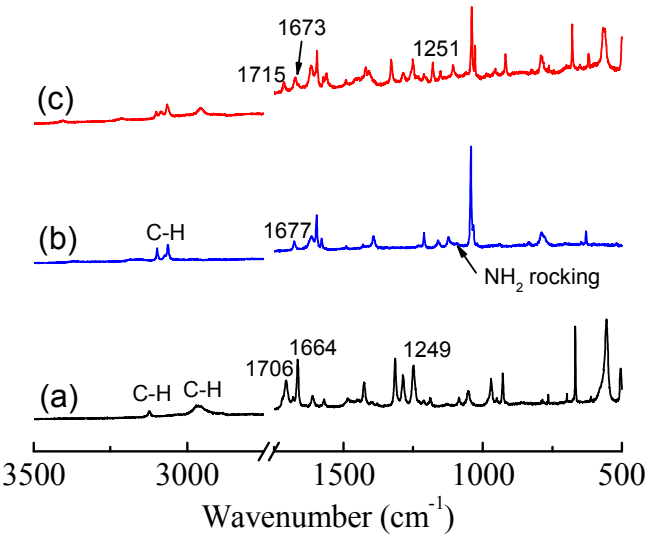

Figure 5 RAMAN spectra of TP (a), NCT (b), and TP-NCT (c).

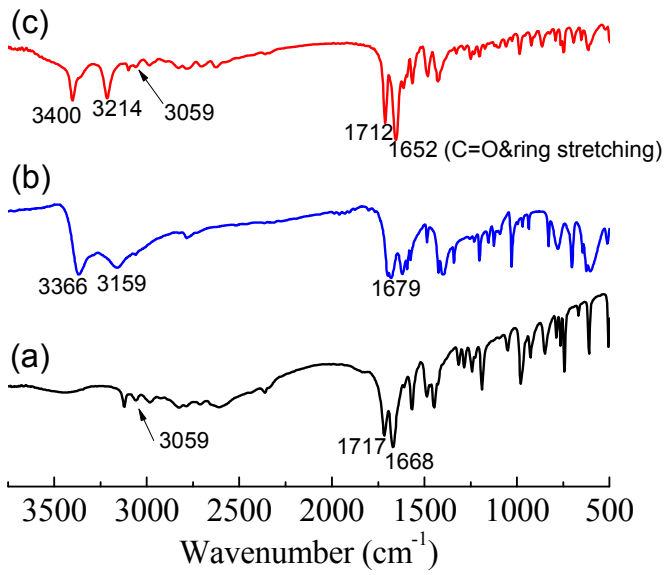

Figure 6 FTIR spectra of TP (a), NCT (b), and TP-NCT (c).

FTIR spectra (Figure 6) show more information about NH and NH_2 groups. After cocrystal formation, the stretching vibration frequency of N4−H remains unchanged[47] (3059 cm^{-1}), indicating the N4−H involved hydrogen bonding does not change significantly (Figure 4). For NCT, asymmetric and symmetric stretching vibrations[48,49] of the $N6H_2$ group at 3366 and 3159 cm^{-1} are blue-shifted to 3407 and 3228 cm^{-1} in the cocrystal, respectively. Such large frequency changes must origin from marked hydrogen bonding structure changes on $N6H_2$ group (Figure 4).

Interpretation of the vibrational data is not straightforward if the crystal structure is not solved. For example, the shifts of the stretching vibrations of $N6H_2$ group should originate from the hydrogen bonding structure changes, rather than the formation/disappearance of hydrogen bonding. Thus, to obtain detailed intermolecular interactions of a powder cocrystal sample, it's more convincing to solve out the crystal structure with credible method, if possible. Several XRPD refined cocrystal structures, such as acyclovir-tartaric acid and adefovir dipivoxil-nicotinamide complexes, have been reported recently.[18,50-52] For the synergistic approach, it was only adopted by Harris for the structure determination of indomethacin-nicotinamide cocrystal.[18] Thus, there must be large space for its wide application in the pharmaceutical crystallography research field.

Conclusions

Crystal structure of the 1:1 theophylline-nicotinamide cocrystal was determined from the powder samples by XRPD refinement. Combined usage with other methods, here 1D solid-state NMR experiments and DFT calculations, the correctness of the refined result was confirmed. The cocrystal mainly adopts an $R_2^2(9)$ supramolecular synthon, which conforms to the hydrogen-bond rules for organic compounds. This study further confirms that supramolecular synthon approach affords a feasible way to design, develop and analyze new pharmaceutical cocrystals, and synergistic approach offers a simple and credible way to solve the crystal structure of powder cocrystal samples.

Acknowledgements

This work was supported by the Natural Science Foundation of China (No. 21205129, 21073226), and Jiangsu Provincial Fund for Natural Sciences (No. BK2012191). The NMR system used in this study was funded through the key scientific equipment plan of the Chinese Academy of Sciences (CAS). Authors also thank FUNSOM, Soochow University, for the calculation supporting.

Notes and references

[a] Laboratory of Magnetic Resonance Spectroscopy and Imaging, Suzhou Institute of Nano-tech and nano-bionics, Chinese Academia of Sciences, Suzhou 215123, P.R. China. Tel: +86-512-62872713; Fax: +86-512-62603079; E-mail: hlzhang2008@sinano.ac.cn.

[b] School of Chemistry and Chemical Engineering, Huazhong University of Science and Technology, Wuhan 430074, P.R. China.

[c] State Key Laboratory of Magnetic Resonance and Atomic and Molecular Physics, Wuhan Institute of Physics and Mathematics, Chinese Academia of Sciences, Wuhan 430071, P.R. China.

[d] Crystal Pharmatech, Suzhou Industrial Park, Suzhou 215123, P.R. China.

[§] These two authors made equal contributions.

† Electronic Supplementary Information (ESI) available: [XRPD patterns, DSC curves, ^{15}N CP/MAS NMR spectra of TP, NCT, and TP-NCT cocrystal. TP-NCT structure after geometry optimization (in CIF format)]. See DOI: 10.1039/b000000x/

1 C. B. Aakeröy and D. J. Salmon, *CrystEngComm*, 2005, **7**, 439.
2 M. J. Zaworotko, *Cryst. Growth Des.*, 2007, **7**, 4.
3 G. R. Desiraju, *CrystEngComm*, 2003, **5**, 466.
4 C. B. Aakeröy, S. Forbes and J. Desper, *J. Am. Chem. Soc.*, 2009, **131**, 17048.
5 V. André, A. Fernandes, P. P. Santos and M. T. Duarte, *Cryst. Growth Des.*, 2011, **11**, 2325.
6 H. D. Clarke, K. K. Arora, H. Bass, P. Kavuru, T. T. Ong, T. Pujari, L. Wojtas and M. J. Zaworotko, *Cryst. Growth Des.*, 2010, **10**, 2152.
7 D. P. McNamara, S. L. Childs, J. Giordano, A. Iarriccio, J. Cassidy, M. S. Shet, R. Mannion, E. O'Donnell and A. Park, *Pharm. Res.*, 2006, **23**, 1888.
8 A. V. Trask, W. D. S. Motherwell and W. Jones, *Cryst. Growth Des.*, 2005, **5**, 1013.
9 G. Springuel and T. Leyssens, *Cryst. Growth Des.*, 2012, **12**, 3374.
10 T. Friščić and W. Jones, *J. Pharm. Pharmacol.*, 2010, **62**, 1547.
11 C. B. Aakeröy, S. Forbes and J. Desper, *CrystEngComm*, 2012, **14**, 2435.
12 S. Karki, L. Fábián, T. Friščić and W. Jones, *Org. Lett.*, 2007, **9**, 3133.
13 K. L. Nguyen, T. Friščić, G. M. Day, L. F. Gladden and W. Jones, *Nat. Mater.*, 2007, **6**, 206.

14 T. Friščić, L. Fabian, J. C. Burley, W. Jones and W. D. S. Motherwell, *Chem. Commun.*, 2006, (48), 5009.
15 E. Y. Cheung, K. D. M. Harris, T. Kang, J. R. Scheffer and J. Trotter, *J. Am. Chem. Soc.*, 2006, **128**, 15554.
16 X. Filip, G. Borodi and C. Filip, *Phy.s Chem. Chem. Phys.*, 2011, **13**, 17978.
17 M. Hušák, A. Jegorov, J. Brus, W. van Beek, P. Pattison, M. Christensen, V. Favre-Nicolin and J. Maixner, *Struct. Chem.*, 2008, **19**, 517.
18 D. V. Dudenko, P. A. Williams, C. E. Hughes, O. N. Antzutkin, S. P. Velaga, S. P. Brown and K. D. M. Harris, *J. Phys. Chem. C*, 2013, **117**, 12258.
19 J. Lu and S. Rohani, *Org. Process Res. Dev.*, 2009, **13**, 1269.
20 M. C. Etter, *Acc. Chem. Res.*, 1990, **23**, 120.
21 H. Wiedenfeld and F. Knoch, *Arch. Pharm.*, 1986, **319**, 654.
22 Z. L. Wang and L. H. Wei, *Acta. Cryst. E*, 2007, **63**, O1681.
23 N. Schultheiss, M. Roe and S. X. M. Boerrigter, *CrystEngComm*, 2011, **13**, 611.
24 S. L. Childs, G. P. Stahly and A. Park, *Mol. Pharmaceutics*, 2007, **4**, 323.
25 M. Bán, P. Bombicz and J. Madarász, *J. Therm. Anal. Calorim.*, 2009, **95**, 895.
26 E. X. Lu, N. Rodriguez-Hornedo and R. Suryanarayanan, *CrystEngComm*, 2008, **10**, 665.
27 A. V. Trask, W. D. S. Motherwell and W. Jones, *Int. J. Pharm.*, 2006, **320**, 114.
28 S. Zaitu, Y. Miwa and T. Taga, *Acta. Cryst. C*, 1995, **51**, 1857.
29 L. S. Rosen, and A. Hybl, *Acta. Cryst. B*, 1971, **27**, 952.
30 P. E. Werner, L. Eriksson and M. Westdahl, *J. Appl. Cryst.*, 1985, **18**, 367.
31 G. S. Pawley, *J. Appl. Cryst.*, 1981, **14**, 357.
32 H. M. Rietveld, *J. Appl. Cryst.*, 1969, **2**, 65.
33 Y. Ebisuzaki, P. D. Boyle and J. A. Smith, *Acta. Cryst. C*, 1997, **53**, 777.
34 Y. Miwa, T. Mizuno, K. Tsuchida, T. Taga and Y. Iwata, *Acta. Cryst. B*, 1999, **55**, 78.
35 A. M. Zheng, S. B. Liu and F. Deng, *J. Comput. Chem.*, 2009, **30**, 222.
36 C. J. Pickard, E. Salager, G. Pintacuda, B. Elena and L. Emsley, *J. Am. Chem. Soc.*, 2007, **129**, 8932.
37 S. J. Clark, M. D. Segall, C. J. Pickard, P. J. Hasnip, M. J. Probert, K. Refson and M. C. Payne, *Z. Kristallogr.*, 2005, **220**, 567.
38 E. D. L. Smith, R. B. Hammond, M. J. Jones, K. J. Roberts, J. B. O. Mitchell, S. L. Price, R. K. Harris, D. C. Apperley, J. C. Cherryman and R. Docherty, *J. Phys. Chem. B*, 2001, **105**, 5818.
39 N. R. Goud, S. Gangavaram, K. Suresh, S. Pal, S. G. Manjunatha, S. Nambiar and A. Nangia, *J. Pharm. Sci.*, 2012, **101**, 664.
40 J. S. Stevens, S. J. Byard and S. L. M. Schroeder, *Cryst. Growth Des.*, 2010, **10**, 1435.
41 M. Majumder, G. Buckton, C. Rawlinson-Malone, A. C. Williams, M. J. Spillman, N. Shankland and K. Shankland, *CrystEngComm*, 2011, **13**, 6327.
42 G. M. Day, J. van de Streek, A. Bonnet, J. C. Burley, W. Jones and W. D. S. Motherwell, *Cryst. Growth Des.*, 2006, **6**, 2301.
43 J. S. Stevens, S. J. Byard, C. A. Muryn and S. L. M. Schroeder, *J. Phys. Chem. B*, 2010, **114**, 13961.
44 K. D. M. Harris and M. C. Xu, Combined analysis of NMR and powder diffraction data. In Harris RK, Wasylishen RE, Duer MJ, editors. NMR crystallography, EMR Books Oxford: Wiley-Blackwell, 2009; pp 275–287.
45 A. S. Tatton, T. N. Pham, F. G. Vogt, D. Iuga, A. J. Edwards and S. P. Brown, *Mol. Pharmaceutics*, 2013, **10**, 999.
46 D. L. Yi, H. L. Zhang and Z. W. Deng, *J. Mol. Catal. A: Chem.*, 2010, **326**, 88.
47 M. M. Nolasco, A. M. Amado and P. J. A. Ribeiro-Claro, *ChemPhysChem*, 2006, **7**, 2150.
48 M. Bakiler, O. Bolukbasi and A. Yilmaz, *J. Mol. Struct.*, 2007, **826**, 6.
49 L. Y. Wang, B. Tan, H. L. Zhang and Z. W. Deng, *Org. Process. Res. Dev.*, 2013, **17**, 1413.
50 Y. Gao, J. Gao, Z. L. Liu, H. L. Kan, H. Zu, W. J. Sun, J. J. Zhang, S. Qian. *Int. J. Pharm.*, 2012, **438**, 327.
51 T. Masuda, Y. Yoshihashi, E. Yonemochi, K. Fujii, H. Uekusa, K. Terada. *Int. J. Pharm.*, 2012, **422**, 160.
52 S. H. Lapidus, A. Lemmerer, J. Bernstein, P. W. Stephens. *Acta. Cryst. C*, 2012, **68**, o335.

Table of Contents Graphic

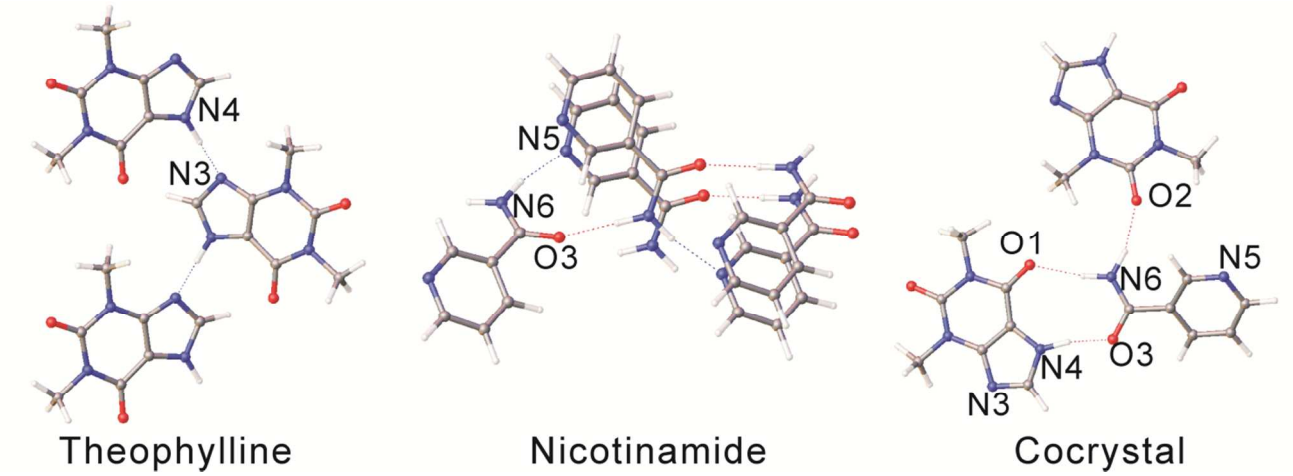

Crystal structure of theophylline-nicotinamide cocrystal is solved for the first time by using a combined multi-technique approach.